

## Article

# UiO-66/Palygorskite/TiO<sub>2</sub> Ternary Composites as Adsorbents and Photocatalysts for Methyl Orange Removal

Thaleia Ioannidou <sup>1</sup>, Maria Anagnostopoulou <sup>2</sup>, Dimitrios Papoulis <sup>3</sup>, Konstantinos C. Christoforidis <sup>1,2,\*</sup>  
and Ioanna A. Vasiliadou <sup>1,\*</sup>

<sup>1</sup> Department of Environmental Engineering, Democritus University of Thrace, 67100 Xanthi, Greece

<sup>2</sup> Institute of Chemistry and Processes for Energy, Environment and Health (ICPEES) UMR7515 CNRS, ECPM, University of Strasbourg, 25 rue Becquerel, CEDEX 2, 67087 Strasbourg, France

<sup>3</sup> Department of Geology, University of Patras, 26504 Patras, Greece

\* Correspondence: kochristo@env.duth.gr (K.C.C.); ioavasil@env.duth.gr (I.A.V.)

**Abstract:** Metal–organic frameworks are recognized as a new generation of emerging porous materials in a variety of applications including adsorption and photocatalysis. The present study presents the development of ternary composite materials made through the coupling of UiO-66 with palygorskite (Pal) clay mineral and titanium dioxide (TiO<sub>2</sub>) applied as adsorbent and photocatalyst for the removal of methyl orange (MO) from aqueous solutions as a typical anionic dye. The prepared materials were characterized using XRD, ATR, DR UV/Vis, and TGA analysis. Detailed kinetic experiments revealed that the presence of the clay at low amounts in the composite outperformed the adsorption efficiency of pure UiO-66, increasing MO adsorption by ca. 8%. In addition, coupling Pal/UiO-66 with TiO<sub>2</sub> for the production of ternary composites provided photocatalytic properties that resulted in complete removal of MO. This was not observed in the pure UiO-66, the Pal/UiO-66 composite, or the pure TiO<sub>2</sub> material. This study presents the first example of clay mineral/MOF/TiO<sub>2</sub> composites with improved performance in removing dyes from aqueous solutions and highlights the importance of coupling MOFs with low-cost clay minerals and photocatalysts for the development of multifunctional advanced composites.

**Keywords:** metal–organic frameworks; UiO-66; palygorskite; anatase; TiO<sub>2</sub>; methyl orange; dye adsorption; dye degradation; photocatalysis



**Citation:** Ioannidou, T.; Anagnostopoulou, M.; Papoulis, D.; Christoforidis, K.C.; Vasiliadou, I.A. UiO-66/Palygorskite/TiO<sub>2</sub> Ternary Composites as Adsorbents and Photocatalysts for Methyl Orange Removal. *Appl. Sci.* **2022**, *12*, 8223. <https://doi.org/10.3390/app12168223>

Academic Editor: Chang-Gu Lee

Received: 19 July 2022

Accepted: 15 August 2022

Published: 17 August 2022

**Publisher's Note:** MDPI stays neutral with regard to jurisdictional claims in published maps and institutional affiliations.



**Copyright:** © 2022 by the authors. Licensee MDPI, Basel, Switzerland. This article is an open access article distributed under the terms and conditions of the Creative Commons Attribution (CC BY) license (<https://creativecommons.org/licenses/by/4.0/>).

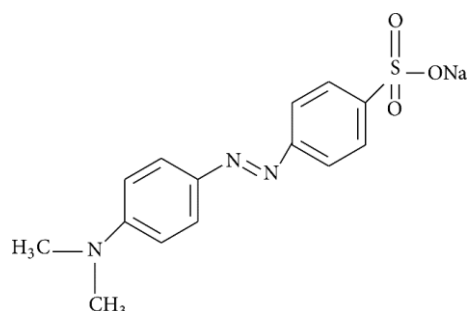
## 1. Introduction

The decrease in environmental quality made clear the need to fill the void between development and sustainability. High amounts of pollutants end up in the aquatic environment [1]. Among the different xenobiotics that enter into the environment, synthetic dyes are a common class of organic pollutants with high concentrations in wastewater since they are used in many different industries (paper, printing, textiles, food, and pharmaceutical industry) [2–5]. Different technologies have been suggested for dye removal from effluents, among which adsorption [6–9] and photocatalysis [10–12] are considered suitable mostly due to the environmentally friendly character of the process. Adsorption offers the benefit of simplicity, high efficiency, and cost-effectiveness. On the other hand, photocatalysis is highly favorable when solid materials are applied as photocatalysts and when solar light is used for the decomposition of organic pollutants.

In both processes, efficiency is driven by the properties of the material used. Regarding adsorption, many different types of materials have been developed and applied in dye removal from the aquatic phase [13–15]. Metal–organic frameworks (MOFs) have been effectively applied as solid absorbing media including dye removal [2,16–21]. MOFs are highly porous synthetic materials that offer the benefit of chemical, textural, and compositional tunability [2]. In addition, they have also been applied as photocatalysts for the

degradation of organic dyes [11,22] and have been coupled efficiently with traditional photocatalysts to improve performance [16,17,23,24] or the development of multifunctional composites [17,25]. Clay minerals have been also extensively studied as adsorbents for dyes removal [19,26,27]. They are low-cost, nontoxic materials with significant cation exchange capacity. However, their negative charge in neutral conditions limits their application as adsorbents of anionic chemical species [28,29]; therefore, chemical modification is required [30,31].

TiO<sub>2</sub> is the most used photocatalyst owing to its inherent properties such as high photocatalytic activity and nontoxicity [32–34]. Among the different polymorphs of TiO<sub>2</sub>, anatase is preferred mostly due to the better charge handling properties [33]. Numerous studies have applied TiO<sub>2</sub>-based materials for the degradation of dyes [35]. Formation of composites through the coupling of TiO<sub>2</sub> with MOF structures has also been exploited in photocatalytic reactions [11,16,17,22,24,25,36]. Clay mineral/TiO<sub>2</sub> composites have also proven to be more active than the individual counter parts in a variety of photocatalytic reactions [37–39]. Since adsorption is a prerequisite for photocatalytic degradation reactions, adsorption of dyes on TiO<sub>2</sub> [40,41] or MOF/TiO<sub>2</sub> composites [42] has also been investigated. As expected, pure TiO<sub>2</sub> materials present much lower adsorption capacity than MOF structures. Recently, Wu et al. showed that coupling MIL-101 (Cr) with TiO<sub>2</sub> increased the adsorption performance against methyl orange (MO) (Scheme 1) [42]. In addition, the adsorption of cationic dyes onto UiO-66/TiO<sub>2</sub> composites was not affected by the presence of TiO<sub>2</sub>, while the composites presented superior photocatalytic activity [25]. Clay/MOF composites have also been developed and studied as adsorbents. However, the effect of the presence of both clay minerals and TiO<sub>2</sub> has never been studied.



**Scheme 1.** Structural formula of methyl orange (MO).

Herein, novel ternary composites bearing UiO-66, palygorskite, and TiO<sub>2</sub> were developed using wet chemical processes. The materials were characterized and tested as adsorbents and photocatalysts for the removal of MO from aqueous solutions. The presence of palygorskite in the composite increased the adsorption efficiency while TiO<sub>2</sub> provided photocatalytic properties able to decompose MO. To the best of our knowledge, such composites made of these particular phases have never been reported before.

## 2. Materials and Methods

All chemicals were used as received without further purification. Palygorskite (Pal, from Ventzia continental basin, Western Macedonia, Greece) was obtained as follows: particles <2 μm were collected by gravity sedimentation, and the clay fraction was separated using centrifugation methods [38,39]. Only the clay fraction of the sample was used for the preparation of the composites in order to avoid other mineral impurities.

### 2.1. Synthesis of UiO-66

Synthesis of UiO-66 (U) was based on a previous reported process [17,43]. Briefly, 1.25 g of zirconium (IV) chloride (ZrCl<sub>4</sub>, 99.5%, Aldrich, Germany) was dissolved in 50 mL of *N,N*-dimethyl formamide (DMF, 99.9%, Aldrich) followed by the addition of 10 mL of acetic acid, forming solution A. On the other hand, 1.23 g of terephthalic acid (Aldrich) was

mixed in 100 mL of DMF, forming solution B. The two solutions were mixed and heated under stirring to 150 °C for 24 h in an oil bath. The material formed was collected by centrifugation and washed three times with ethanol and with acetone. Solvent exchange with acetone was performed over a period of 4 days. The solvent was changed every second day. Finally, the material was dried at 100 °C over night and stored in a desiccator.

## 2.2. Synthesis of TiO<sub>2</sub>

Anatase TiO<sub>2</sub> (T) was synthesized using the microemulsion process [44]. Titanium(IV) isopropoxide (Aldrich, Germany) was added to an inverse emulsion of 50 mL of water and *n*-heptane (85/10 *v/v* vs. H<sub>2</sub>O). The water/Ti molar ratio was equal to 100. Triton X-100 was used as a surfactant in 1-hexanol (105/100 *v/v* vs. surfactant). The solution was stirred for 24 h at room temperature. The material was collected and washed thoroughly with methanol by centrifugation and dried at 110 °C overnight. Anatase TiO<sub>2</sub> was obtained by calcination for 2 h at static air and 400 °C using a ramp of 1 °C·min<sup>-1</sup>.

## 2.3. Synthesis of Binary Palygorskite/UiO-66 Composite

For the development of the palygorskite/UiO-66 composite (PU), a similar synthesis process was used with a slide modification. Firstly, 0.1 g of palygorskite was added to the ZrCl<sub>4</sub> solution, and the amounts of ZrCl<sub>4</sub> and terephthalic acid were adjusted, keeping the same ratio, such that the final composite contained a theoretical nominal amount of 10% by weight of palygorskite. The same washing and activation process was used as in the U sample.

## 2.4. Synthesis of Palygorskite/UiO-66/TiO<sub>2</sub> Composite

The Pal/UiO-66/TiO<sub>2</sub> ternary composite (PUT) was developed using a facile wet impregnation method. Preformed PU and TiO<sub>2</sub> were mixed at a mass ratio equal to 6/4 in 100 mL of double-distilled water. The mixture was first sonicated for 30 min and then stirred overnight. Mixing was followed by removing the solvent using rotary evaporation, drying overnight at 100 °C, and a thermal treatment step at 200 °C for 4 h (ramp 1 °C·min<sup>-1</sup>).

## 2.5. Materials Characterization

X-ray diffraction (XRD) measurements were performed using a Bruker D8-Advance diffractometer equipped with a Lynx Eye detector operating at 40 kV and 40 mA, using K<sub>α</sub> radiation of Cu at 1.5418°. A Thermo Fisher Nicolet iS10 spectrometer was used to obtain the attenuated total reflectance (ATR) IR spectrum in the 400–4000 cm<sup>-1</sup> range. Thermogravimetric analysis (TGA) was performed using a TA Instrument Q5000IR. Each sample was heated under air flow (25 mL·min<sup>-1</sup>) up to 650 °C with a dynamic ramping rate depending on the weight loss. Diffuse reflectance UV/Vis absorption spectra were recorded in the range of 200–800 nm using a PerkinElmer Lambda 950 Scan spectrophotometer equipped with integrating sphere. For this analysis, BaSO<sub>4</sub> was used as the reference. An X-band Bruker ER200D electron paramagnetic resonance (EPR) spectrometer operating at the X-band frequencies was used to perform spin trap experiments. The 5,5-dimethyl-1-pyrroline *N*-oxide (DMPO) was used as spin trap for the detection of hydroxyl radicals (OH•) at room temperature. A suspension of 1 mg·mL<sup>-1</sup> of the catalyst in water was sonicated for 10 min. Then, 100 μL of the above suspension was mixed with 100 μL of 0.005 M DMPO directly in the EPR flat cell. A quartz EPR flat cell was used.

## 2.6. Adsorption Experiments

The material (20 mg) was placed in an Erlenmeyer flask containing 50 mL of 90 mg·L<sup>-1</sup> MO aqueous solution. The pH of the suspension was adjusted to 5. Adsorption experiments were performed in a temperature-controlled incubator. The temperature was maintained at 25 °C, and the adsorption process was performed under dark conditions throughout the whole experiment. For the preparation of all solutions, Milli-Q water was used. Adsorption of MO was quantified through the following process; aliquots of 1.5 mL were periodically

taken, filtered using a 0.45  $\mu\text{m}$  PTFE Millipore disc, and measured using a Varian Cary 100 Scan spectrophotometer. Quantification of MO was based on comparison with standards. The adsorption capacity evaluation was performed using the following equation:

$$q_e = \frac{(C_0 - C_e) \times V}{m}, \quad (1)$$

where  $q_e$  ( $\text{mg} \cdot \text{g}^{-1}$ ) is the adsorbed amount at equilibrium,  $C_0$  and  $C_e$  ( $\text{mg} \cdot \text{L}^{-1}$ ) are the initial dye concentrations and at equilibrium, respectively,  $V$  is the volume of the mixture (mL), and  $m$  is the mass of the adsorbent (mg). The removal efficiency was calculated using the following equation:

$$\text{RE} = \frac{(C_0 - C_e) \times 100}{C_0}. \quad (2)$$

### 2.7. Photocatalytic Reactions

Photocatalytic tests were carried out after the adsorption process reached equilibrium. In brief, after incubating the material with the MO solution under dark conditions for 1.5 h, the mixture was irradiated using six UV lamps (Philips 24W/10/4P lamps,  $\lambda_{\text{max}} = 365$  nm) symmetrically positioned in the periphery of the photoreactor. The temperature of the mixture was maintained at 25 °C with water circulation by means of a cryostat. Reactions were performed at ambient pressure. Samples were periodically taken and filtered using a 0.45  $\mu\text{m}$  PTFE Millipore disc. The UV/Vis spectra were then collected using a Varian Cary 100 Scan spectrophotometer.

### 2.8. Recycling of the Materials

Recycling was performed by redispersing the materials in water at pH 10 to accelerate the desorption process followed by sonication for 10 min and washing thoroughly via centrifugation until pH was neutral. Then, the material was washed ethanol three times and finally dried at 100 °C under vacuum for 5 h.

## 3. Results and Discussion

### 3.1. Materials Characterization

Structural information of the prepared materials was first obtained by means of X-ray diffraction (XRD) analysis. Figure 1 presents the diffraction patterns of all materials. A typical diffraction pattern for the pure UiO-66 was observed [25,45]. The PU composite presented the same diffraction pattern as the U sample. This observation verified that the presence of Pal did not affect the synthesis of UiO-66. No diffraction peak attributed to Pal was detected in the PU sample. Two reasons are probably responsible for this. Firstly, the amount of Pal in the composite was small. Secondly, there was an intense diffraction peak from UiO-66 in the ca. 8.5° region that overlapped with the main diffraction peak of Pal.  $\text{TiO}_2$  presented the typical diffraction pattern of anatase. The PUT composite had a diffraction pattern that was a combination of the pure UiO-66 and  $\text{TiO}_2$  sample, without any obvious differences compared with the patterns of their pure counterparts.

The materials were further characterized using attenuated total reflection Fourier-transform infrared (ATR-FTIR) spectroscopy, and the data are given in Figure 2a. The characteristic peaks of UiO-66 were observed in the materials containing this specific MOF (U, PU, and PUT) [46–48]. The symmetric and asymmetric stretch vibrations in the  $\text{COO}^-$  group of the organic linker were observed at 1392  $\text{cm}^{-1}$  and 1582  $\text{cm}^{-1}$ , while the vibrational mode of the C=C bond in the benzene ring was centered at 1510  $\text{cm}^{-1}$ . Vibrational modes of the C–H, C=C, O–H, and OCO bonds were detected in the region 810–710  $\text{cm}^{-1}$ . The broad peak at the beginning of the spectra (400–800  $\text{cm}^{-1}$ ) was attributed to the presence of  $\text{TiO}_2$  [44,49]. Regarding the Pal sample, an intense peak was observed in the region 97–1060  $\text{cm}^{-1}$ . This was not observed in the pure UiO-66 sample but was present in all composites bearing Pal (i.e., PU and PUT). This peak was attributed to the Si–O–Mg asymmetric stretching vibration [39,46,50] and verified the presence of Pal in the composite

materials. It should be noted that the peak centered at  $1582\text{ cm}^{-1}$  in the UiO-66 sample was shifted to higher wavenumbers in the composite samples bearing Pal (Figure 2b). This is probably linked with the in-situ development of UiO-66 in the presence of Pal and suggests an interaction of the clay mineral with the carboxylate groups of the organic linker in the MOF structure. Overall, ATR verified the presence of UiO-66, Pal, and  $\text{TiO}_2$  in the composite materials.

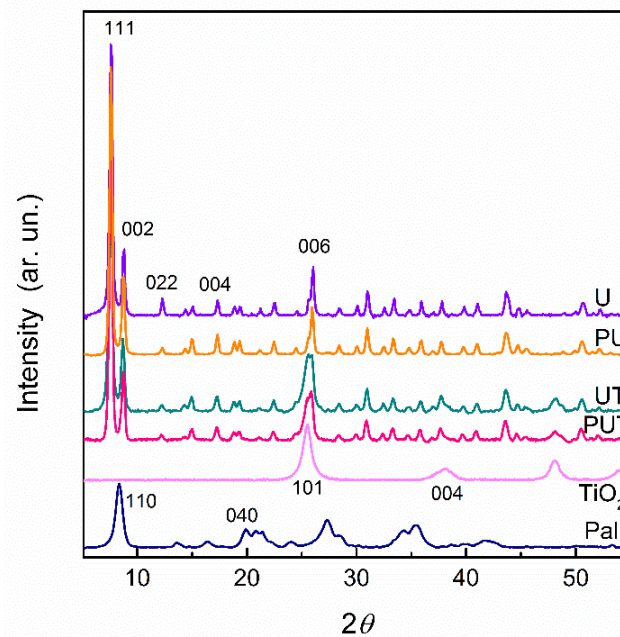


**Figure 1.** XRD patterns of the pure and composite materials.

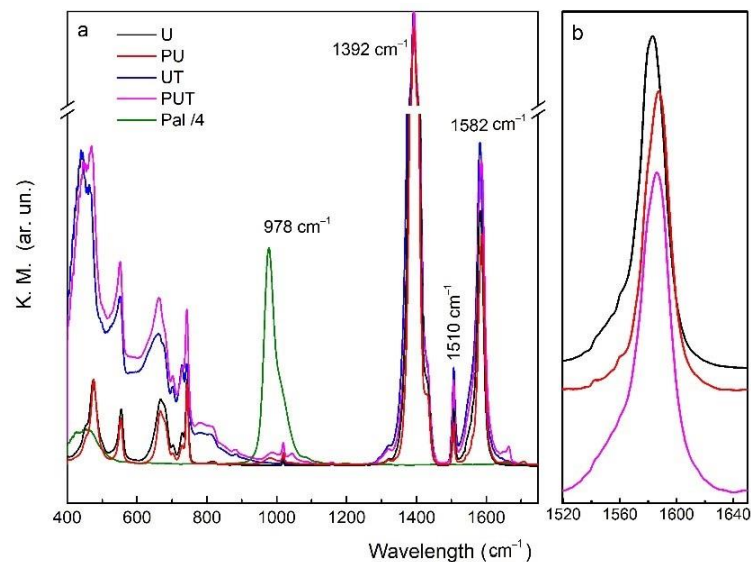


**Figure 2.** ATR spectra of all prepared materials (a); zoomed area of the COO-group vibration mode (b).

In order to get information regarding the amount of the different parts in the composites, the prepared materials were subjected to thermogravimetric (TGA) analysis. The TGA profiles of all materials are illustrated in Figure 3. A smooth mass decrease was observed in the pure  $\text{TiO}_2$  that ended at ca. 7% total mass loss at  $550\text{ }^\circ\text{C}$ . The mass loss was greater in the Pal sample (ca. 18% at  $550\text{ }^\circ\text{C}$ ). In this temperature range, the mass loss in the Pal sample was attributed to both superficially adsorbed and loosely bound zeolitic water, as well as structural  $\text{OH}_2$  [51,52]. In the materials containing UiO-66, the small

weight loss in the temperature range 50–400 °C was due to the loss of guest molecules (DMF). The fast drop in mass loss at temperatures higher than 450 °C was attributed to the decomposition of the organic framework of UiO-66. This second drop in mass was observed at lower temperatures in the composite bearing TiO<sub>2</sub>. Taking into account the mass loss in the composites at temperatures higher than 400 °C (indicated by  $\Delta$ mass in Figure 3 for sample U) and the corresponding weight loss in the pure Pal and TiO<sub>2</sub>, the Pal content was calculated equal to 7 wt.% in the PU and PUT samples, and the TiO<sub>2</sub> content was calculated equal to 39 wt.% in the PUT composite.

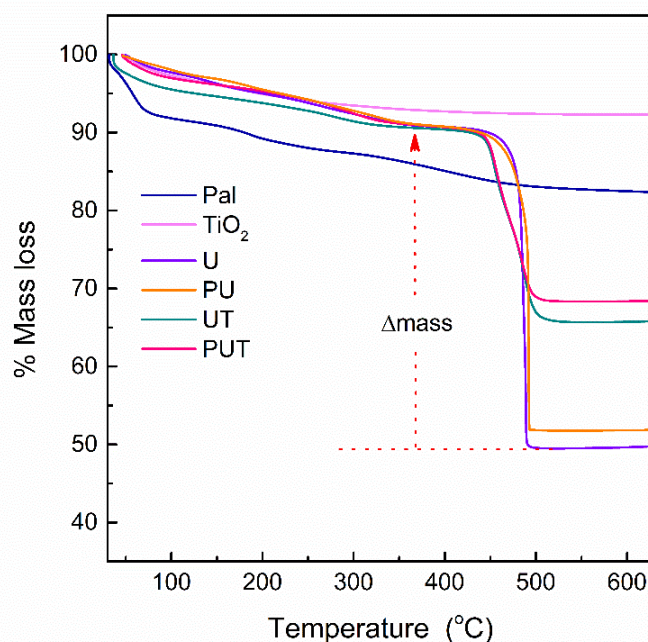


**Figure 3.** TGA profiles of the pure Pal and TiO<sub>2</sub> samples and the prepared U, PU, and PUT materials.

Diffuse reflectance UV/Vis spectroscopy was applied to study the electronic properties related with light absorption. Figure 4a presents the UV/Vis absorption spectra of the materials. The corresponding Tauc plots [38,39,53] used to estimate the bandgap energies ( $E_g$ ) are given in Figure 4b. Materials containing TiO<sub>2</sub> were treated as direct, while the remaining materials were treated as indirect semiconductors [17]. Pure UiO-66 absorbed light at wavelengths lower than 310 nm in accordance with the literature [24]. The same absorption onset was observed for the PU sample. This corresponded to  $E_g$  values of ca. 4 eV. The absorption edge of TiO<sub>2</sub> was observed at ca. 390 nm, while Pal absorbed light in the whole visible region [38,39]. Light absorption of the composites was a combination of the absorption of the individual counter parts. The absorption onset of the PUT material was observed at ca. 390 nm, as for the pure TiO<sub>2</sub>. This corresponded to an  $E_g$  value of 3.18 eV, typical for pure anatase TiO<sub>2</sub> [16]. A broad absorption was observed in visible region (400–800 nm) for both PU and PUT samples. This was strictly attributed to the presence of Pal. Overall, it was verified through DR UV/Vis spectroscopy that all parts in the composite contributed to the light absorption properties of the material.

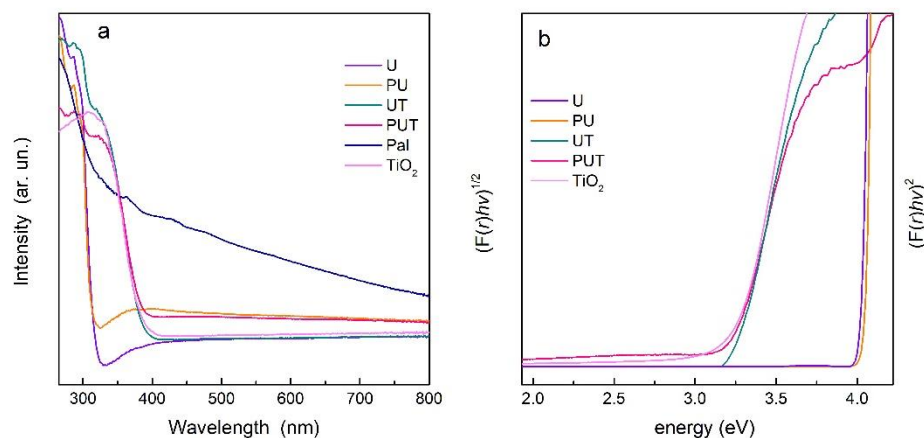


**Figure 4.** UV/Vis absorption spectra (a) and plots used to estimate the bandgap energies (b).

### 3.2. Dye Adsorption Evaluation

The effect of contact time on MO adsorption over the prepared materials is given in Figure 5a. Adsorption equilibrium was achieved within less than 5 min for all materials containing UiO-66. On the contrary, equilibrium was reached at longer reaction times for pure Pal and TiO<sub>2</sub>. Significant differences were also detected in the experimentally observed adsorption capacity at equilibrium ( $q_{e,exp}$ ). The  $q_{e,exp}$  together with the removal efficiency (RE %) are given in Table 1. Both TiO<sub>2</sub> and Pal presented low  $q_e$  and removal efficiency. On the contrary, the pure U and PU composite presented high adsorption capacity, with the PU sample being the most efficient ( $q_e = 213.3 \text{ mg}\cdot\text{g}^{-1}$ ). This suggests that the presence of Pal at low amounts in the composite was beneficial for MO adsorption. An increase in the adsorption capacity of dyes was previously shown in oxide/MOFs or clay mineral/MOF composites including UiO-66 [25,42,54,55], as well as in other MOF-based composites [20,21]. In the specific case of Pal/UiO-66 composites, formation of microporosity at the interface of the two parts was shown to increase the specific surface area that may affect adsorption efficiency [56]. A decrease in the  $q_e$  and the removal efficiency was observed in the composite bearing TiO<sub>2</sub> (i.e., PUT). This was probably related to the relatively high amount of TiO<sub>2</sub> in the PUT composite that presented low  $q_e$ . However, the removal efficiency in these composites was not a linear combination of the individual counter parts considering their content in the composites. Taking into account the fast kinetic profile of MO adsorption, the high  $q_e$ , and the removal efficiency, the adsorption behavior of the PUT composite was dominated by UiO-66. Lastly, in order to verify the stability of the composites, recycling adsorption experiments using the most efficient composite were performed (Figure S1). The stability was evidenced by the small loss of adsorption efficiency after three consecutive cycles [56].

**Table 1.** Experimentally obtained and calculated values for  $q_e$ , removal efficiency (RE %), and correlation coefficient ( $R^2$ ) for the pseudo-second-order kinetic model used to simulate the adsorption process and photocatalytic rate constant ( $k$ ).

Sample	$q_{e,exp}$ ( $\text{mg}\cdot\text{g}^{-1}$ )	RE (%) <sup>1</sup>	$q_{e,cal}$ ( $\text{mg}\cdot\text{g}^{-1}$ )	$k_2$ ( $\text{g}\cdot\text{mg}^{-1}\cdot\text{min}^{-1}$ ) <sup>2</sup>	$R^2$	$k$ ( $\text{min}^{-1}$ ) <sup>3</sup>
U	195.7	87.1	196.1	0.012	0.999	
PU	213.3	94.9	212.8	0.074	0.999	
PUT	174.7	77.5	175.4	0.108	0.999	0.0153
TiO <sub>2</sub>	41.3	18.3				0.0043
Pal	20.9	9.3				

<sup>1</sup> Removal efficiency; <sup>2</sup>  $k_2$ : rate constant of the second-order adsorption kinetics; <sup>3</sup>  $k$ : first-order rate constant of the photocatalytic removal of MO.

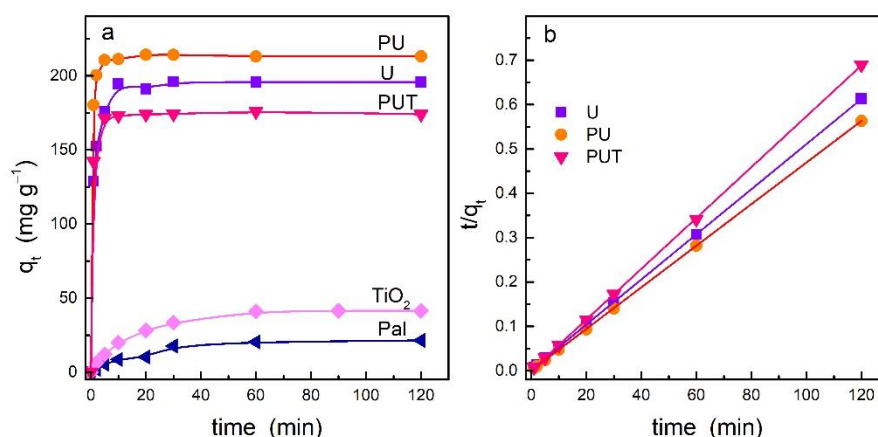


**Figure 5.** Time dependence of MO adsorption on the pure Pal,  $\text{TiO}_2$ , and UiO-66 and the prepared composites (PU and PUT) (a). Pseudo-second-order rate law for MO adsorption on materials containing UiO-66 (b). Experimental conditions:  $90 \text{ mg}\cdot\text{L}^{-1}$  initial MO concentration,  $0.4 \text{ g}\cdot\text{L}^{-1}$  of the adsorbent,  $\text{pH} = 5$ , volume = 50 mL, and  $T = 25^\circ\text{C}$ .

The pseudo-second-order kinetic model [54,55,57–59] was used to fit the experimental data as represented by Equation (3).

$$\frac{t}{q_t} = \frac{1}{k_2 q_e^2} + \frac{t}{q_e}, \quad (3)$$

where  $q_e$  is the amount of MO adsorbed at equilibrium,  $q_t$  the MO adsorbed at time  $t$ , and  $k_2$  is the rate constant ( $\text{g}\cdot\text{mg}^{-1}\cdot\text{min}^{-1}$ ) of the second-order adsorption kinetics. The fitted adsorption kinetic curves for the materials containing UiO-66 as a function of time are given in Figure 5b. The correlation coefficient  $R^2$  together with the calculated adsorption at equilibrium ( $q_{e,\text{cal}}$ ) is given in Table 1. High correlation coefficients were obtained for all materials. In addition,  $q_{e,\text{cal}}$  matched the experimental observation. These findings indicate that MO adsorption onto the pure U sample and all composites containing UiO-66 followed the pseudo-second-order kinetic model [54,55,57,58]. Overall, the adsorption experiments showed that Pal induced an increase in MO adsorption, while the presence of ca. 40 wt.%  $\text{TiO}_2$  did not significantly affect the adsorption given its relatively high content in the composite and the low adsorption capacity.

### 3.3. Photocatalytic Activity Evaluation

The materials were further tested as photocatalysts for the degradation of MO. Before starting the catalytic process, the mixture containing  $90 \text{ mg}\cdot\text{L}^{-1}$  MO and 20 mg of the material was stirred in dark conditions for 1.5 h, as indicated by the adsorption experiments. The shaded area in Figure 6a corresponds to the adsorption process. After adsorption/desorption equilibrium was achieved, the sample was irradiated with UV light. The kinetics of MO photocatalytic degradation was monitored for 2 h. The data are presented in Figure 6a. No obvious decrease in MO concentration was detected by the Pal, pure UiO-66, and PU composite. Clay minerals do not possess any photocatalytic activity. On the contrary, UiO-66 is photoactive [37,53]. However, on the basis of the U and PU light absorption properties (Figure 4), light irradiation at wavelengths lower than 310 nm was required for their activation. Therefore, it is not surprising that U and PU were not active under the conditions of our experiment. MO concentration was reduced when materials containing  $\text{TiO}_2$  were used. This implies that PUT is photoactive and able to degrade MO. UiO-66/ $\text{TiO}_2$  composites were previously proven to be active in photocatalytic degradation of dyes [25,60]. Pure  $\text{TiO}_2$  removed approximately 50% of the initial MO. Comparing the materials presenting photoactivity, complete decolorization was achieved only in the PUT composite within less than 2 h irradiation. The composite bearing UiO-66 and  $\text{TiO}_2$  (UT) also presented photoactivity, but the removal efficiency was lower than that of the PUT

composite. The high removal efficiency of PUT against MO was linked to both functions of the PUT composite (i.e., adsorbent and photocatalyst). Most of the MO (77.5%) was adsorbed, while the remainder was decomposed via photocatalysis.

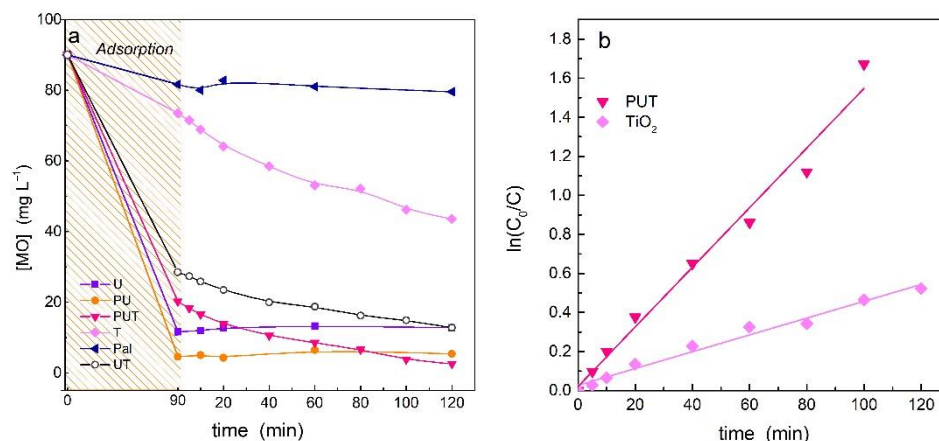


**Figure 6.** Photocatalytic removal of MO following the adsorption process (a) and the corresponding first-order kinetic plots (b). Experimental conditions: 90 mg·L<sup>-1</sup> initial MO concentration, 0.4 g·L<sup>-1</sup> of the material, pH = 5, volume = 50 mL, T = 25 °C, and adsorption period = 1.5 h.

In order to further evaluate the photocatalytic efficiency of the prepared materials, the photocatalytic degradation rates were calculated. The data were well fitted with a first-order kinetic model. Rate constants (*k*) were estimated by fitting the experimental data with the following equation:

$$\ln \frac{C_0}{C} = kt, \quad (4)$$

where *k* is the apparent first-order rate constant (min<sup>-1</sup>), *t* is the irradiation time (min), *C*<sub>0</sub> is the initial concentration (i.e., after the adsorption/desorption process reached equilibrium), and *C* is the concentration of MO at reaction time *t*. The data are presented in Figure 6b, and the photocatalytic degradation rates (*k*) are summarized in Table 1. The PUT composite presented higher degradation rates than the pristine TiO<sub>2</sub>. This has previously been seen in UiO-66/TiO<sub>2</sub> [24,60] composites, as well as in clay/TiO<sub>2</sub> or TiO<sub>2</sub>-based composites containing other natural porous minerals [37–39,61].

The improved photoactivity in TiO<sub>2</sub> composites has been linked with synergistic effects related to the increase in charge availability [11,25,45], as well as the deposition of TiO<sub>2</sub> nanoparticles on the support, which decreases agglomeration phenomena [37,39]. Both factors are important for photocatalytic reactions in the liquid phase [12]. An additional contributor to the improved photoactivity was the increase in the contact between TiO<sub>2</sub> and the substrate [17,53]. This could be achieved through the increase in MO concentration close to TiO<sub>2</sub> due to the high adsorption efficiency of UiO-66. The large size of MO molecular structure and the fast adsorption kinetics suggest that MO was most likely adsorbed onto the external surface of UiO-66 where TiO<sub>2</sub> particles were present. This potentially increased the contact between TiO<sub>2</sub> and MO, improving photoactivity.

To further verify the photocatalytic activity of the composites, in situ spin-trap electron paramagnetic resonance (EPR) spectroscopy was performed using DMPO to study the reactive oxygen species formed under irradiation. Figure 7 presents the EPR spectrum obtained at room temperature after 15 min irradiation of a PUT aqueous suspension under light irradiation conditions identical to the photocatalytic experiments. An EPR signal with a 1:2:2:1 intensity ratio corresponding to the DMPO–OH• spin adduct was observed. These data clearly indicate that the PUT composite was able to produce OH• under irradiation. A similar analysis was performed for the PU composite. However, no DMPO–OH• was detected (Figure 7). This suggests that TiO<sub>2</sub> was required in the composite

to produce reactive oxygen species. These data may explain the inability of PU and pure U to decompose MO under the conditions of our experiment.

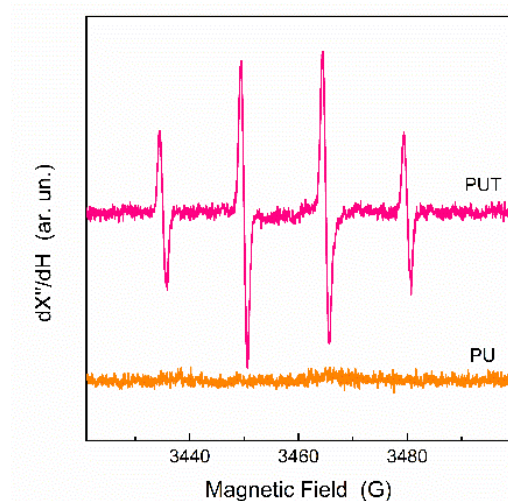


**Figure 7.** Room temperature DMPO spin-trapping EPR spectra of the PUT and PU composites in aqueous suspensions under 15 min of light irradiation.

#### 4. Conclusions

A facile two-step synthesis process was applied for the synthesis of clay mineral/MOF/TiO<sub>2</sub> ternary composites as adsorbents and photocatalysts for the removal of MO from aqueous solutions. Pure Pal and TiO<sub>2</sub> presented low adsorption capacities. Low amounts of Pal in the composite increased adsorption by ca. 8%. The presence of TiO<sub>2</sub> at 40 wt.% reduced the adsorption efficiency but not significantly. In addition, it induced photocatalytic properties in the composite. Materials made of Pal, UiO-66, and TiO<sub>2</sub> completely removed MO, while pure TiO<sub>2</sub> removed ca. 50% of the initial dye concentration. This study highlights the importance of composites for the development of efficient materials presenting multifunctionality and presents the first example of coupling UiO-66 with low-cost clay minerals and TiO<sub>2</sub> for the development of dual-function advanced materials.

**Supplementary Materials:** The following supporting information can be downloaded at <https://www.mdpi.com/article/10.3390/app12168223/s1>: Figure S1. Percentage removal efficiency of MO by the PU composite over three consecutive cycles.

**Author Contributions:** Conceptualization, I.A.V.; methodology, K.C.C. and I.A.V.; validation, I.A.V., K.C.C., and D.P.; formal analysis, I.A.V.; investigation, T.I., M.A., and I.A.V.; resources, I.A.V., K.C.C., and D.P.; data curation, I.A.V. and K.C.C.; writing—original draft preparation, I.A.V.; writing—review and editing, I.A.V. and K.C.C.; visualization, I.A.V. and M.A.; supervision, I.A.V. and K.C.C.; project administration, I.A.V. and K.C.C.; funding acquisition, K.C.C. and I.A.V. All authors have read and agreed to the published version of the manuscript.

**Funding:** This work benefited from state aid managed by the French National Research Agency (ANR) under the Investments for the Future (program “Make Our Planet Great Again”) with reference ANR-18-MOPGA-0014. The research was partially funded by Democritus University of Thrace (project 82268).

**Conflicts of Interest:** The authors declare no conflict of interest.

#### References

1. Saravanan, A.; Kumar, P.S.; Yaashikaa, P.R.; Karishma, S.; Jeevanantham, S.; Swetha, S. Mixed Biosorbent of Agro Waste and Bacterial Biomass for the Separation of Pb(II) Ions from Water System. *Chemosphere* **2021**, *277*, 130236. [[CrossRef](#)] [[PubMed](#)]
2. Uddin, M.J.; Ampiauw, R.E.; Lee, W. Adsorptive Removal of Dyes from Wastewater Using a Metal-Organic Framework: A Review. *Chemosphere* **2021**, *284*, 131314. [[CrossRef](#)] [[PubMed](#)]

3. Murugesan, A.; Loganathan, M.; Senthil Kumar, P.; Vo, D.-V.N. Cobalt and Nickel Oxides Supported Activated Carbon as an Effective Photocatalysts for the Degradation Methylene Blue Dye from Aquatic Environment. *Sustain. Chem. Pharm.* **2021**, *21*, 100406. [[CrossRef](#)]
4. Renita, A.A.; Vardhan, K.H.; Kumar, P.S.; Nguéagni, P.T.; Abilarasu, A.; Nath, S.; Kumari, P.; Saravanan, R. Effective Removal of Malachite Green Dye from Aqueous Solution in Hybrid System Utilizing Agricultural Waste as Particle Electrodes. *Chemosphere* **2021**, *273*, 129634. [[CrossRef](#)] [[PubMed](#)]
5. Jiang, D.; Chen, M.; Wang, H.; Zeng, G.; Huang, D.; Cheng, M.; Liu, Y.; Xue, W.; Wang, Z. The Application of Different Typological and Structural MOFs-Based Materials for the Dyes Adsorption. *Coord. Chem. Rev.* **2019**, *380*, 471–483. [[CrossRef](#)]
6. Abhinaya, M.; Parthiban, R.; Kumar, P.S.; Vo, D.-V.N. A Review on Cleaner Strategies for Extraction of Chitosan and Its Application in Toxic Pollutant Removal. *Environ. Res.* **2021**, *196*, 110996. [[CrossRef](#)] [[PubMed](#)]
7. Sharma, G.; AlGarni, T.S.; Kumar, P.S.; Bhogal, S.; Kumar, A.; Sharma, S.; Naushad, M.; AlOthman, Z.A.; Stadler, F.J. Utilization of Ag<sub>2</sub>O–Al<sub>2</sub>O<sub>3</sub>–ZrO<sub>2</sub> Decorated onto RGO as Adsorbent for the Removal of Congo Red from Aqueous Solution. *Environ. Res.* **2021**, *197*, 111179. [[CrossRef](#)]
8. Ullah, S.; Al-Sehemi, A.G.; Mubashir, M.; Mukhtar, A.; Saqib, S.; Bustam, M.A.; Cheng, C.K.; Ibrahim, M.; Show, P.L. Adsorption Behavior of Mercury over Hydrated Lime: Experimental Investigation and Adsorption Process Characteristic Study. *Chemosphere* **2021**, *271*, 129504. [[CrossRef](#)]
9. Yang, R.; Li, D.; Li, A.; Yang, H. Adsorption Properties and Mechanisms of Palygorskite for Removal of Various Ionic Dyes from Water. *Appl. Clay Sci.* **2018**, *151*, 20–28. [[CrossRef](#)]
10. Christoforidis, K.C.; Montini, T.; Bontempi, E.; Zafeiratos, S.; Jaén, J.J.D.; Fornasiero, P. Synthesis and Photocatalytic Application of Visible-Light Active  $\beta$ -Fe<sub>2</sub>O<sub>3</sub>/g-C<sub>3</sub>N<sub>4</sub> Hybrid Nanocomposites. *Appl. Catal. B Environ.* **2016**, *187*, 171–180. [[CrossRef](#)]
11. Dias, E.M.; Petit, C. Towards the Use of Metal–Organic Frameworks for Water Reuse: A Review of the Recent Advances in the Field of Organic Pollutants Removal and Degradation and the next Steps in the Field. *J. Mater. Chem. A* **2015**, *3*, 22484–22506. [[CrossRef](#)]
12. Akpan, U.G.; Hameed, B.H. Parameters Affecting the Photocatalytic Degradation of Dyes Using TiO<sub>2</sub>-Based Photocatalysts: A Review. *J. Hazard. Mater.* **2009**, *170*, 520–529. [[CrossRef](#)]
13. Salleh, M.A.M.; Mahmoud, D.K.; Karim, W.A.W.A.; Idris, A. Cationic and Anionic Dye Adsorption by Agricultural Solid Wastes: A Comprehensive Review. *Desalination* **2011**, *280*, 1–13. [[CrossRef](#)]
14. Cheung, W.H.; Szeto, Y.S.; McKay, G. Enhancing the Adsorption Capacities of Acid Dyes by Chitosan Nano Particles. *Bioresour. Technol.* **2009**, *100*, 1143–1148. [[CrossRef](#)] [[PubMed](#)]
15. Belaid, K.D.; Kacha, S.; Kameche, M.; Derriche, Z. Adsorption Kinetics of Some Textile Dyes onto Granular Activated Carbon. *J. Environ. Chem. Eng.* **2013**, *1*, 496–503. [[CrossRef](#)]
16. Crake, A.; Christoforidis, K.C.; Gregg, A.; Moss, B.; Kafizas, A.; Petit, C. The Effect of Materials Architecture in TiO<sub>2</sub> /MOF Composites on CO<sub>2</sub> Photoreduction and Charge Transfer. *Small* **2019**, *15*, 1805473. [[CrossRef](#)]
17. Crake, A.; Christoforidis, K.C.; Kafizas, A.; Zafeiratos, S.; Petit, C. CO<sub>2</sub> Capture and Photocatalytic Reduction Using Bifunctional TiO<sub>2</sub>/MOF Nanocomposites under UV–Vis Irradiation. *Appl. Catal. B Environ.* **2017**, *210*, 131–140. [[CrossRef](#)]
18. Au, V.K.-M. Recent Advances in the Use of Metal–Organic Frameworks for Dye Adsorption. *Front. Chem.* **2020**, *8*, 708. [[CrossRef](#)]
19. Ramírez, D.J.; Alfonso Herrera, L.A.; Colorado-Peralta, R.; Rodríguez, R.P.; Camarillo Reyes, P.K.; Chiñas, L.E.; Sánchez, M.; Rivera, J.M. Highly Efficient Methyl Orange Adsorption by UV-012, a New Crystalline Co<sup>II</sup> MOF. *CrystEngComm* **2021**, *23*, 3537–3548. [[CrossRef](#)]
20. Cheng, J.; Liu, K.; Li, X.; Huang, L.; Liang, J.; Zheng, G.; Shan, G. Nickel-Metal–Organic Framework Nanobelt Based Composite Membranes for Efficient Sr<sup>2+</sup> Removal from Aqueous Solution. *Environ. Sci. Ecotechnology* **2020**, *3*, 100035. [[CrossRef](#)]
21. Cheng, J.; Liang, J.; Dong, L.; Chai, J.; Zhao, N.; Ullah, S.; Wang, H.; Zhang, D.; Imtiaz, S.; Shan, G.; et al. Self-Assembly of 2D-Metal–Organic Framework/Graphene Oxide Membranes as Highly Efficient Adsorbents for the Removal of Cs<sup>+</sup> from Aqueous Solutions. *RSC Adv.* **2018**, *8*, 40813–40822. [[CrossRef](#)] [[PubMed](#)]
22. Mansouri, M.; Sadeghian, S.; Mansouri, G.; Setareshenas, N. Enhanced Photocatalytic Performance of UiO-66-NH<sub>2</sub>/TiO<sub>2</sub> Composite for Dye Degradation. *Environ. Sci. Pollut. Res.* **2021**, *28*, 25552–25565. [[CrossRef](#)] [[PubMed](#)]
23. Liu, Z.; Zhuang, Y.; Dong, L.; Mu, H.; Tian, S.; Wang, L.; Huang, A. Preparation of CeO<sub>2</sub>/UiO-66-NH<sub>2</sub> Heterojunction and Study on a Photocatalytic Degradation Mechanism. *Materials* **2022**, *15*, 2564. [[CrossRef](#)] [[PubMed](#)]
24. Man, Z.; Meng, Y.; Lin, X.; Dai, X.; Wang, L.; Liu, D. Assembling UiO-66@TiO<sub>2</sub> Nanocomposites for Efficient Photocatalytic Degradation of Dimethyl Sulfide. *Chem. Eng. J.* **2022**, *431*, 133952. [[CrossRef](#)]
25. Wang, Y.; Liu, H.; Zhang, M.; Duan, W.; Liu, B. A Dual-Functional UiO-66/TiO<sub>2</sub> Composite for Water Treatment and CO<sub>2</sub> Capture. *RSC Adv.* **2017**, *7*, 16232–16237. [[CrossRef](#)]
26. Abidi, N.; Errais, E.; Duplay, J.; Berez, A.; Jrad, A.; Schäfer, G.; Ghazi, M.; Semhi, K.; Trabelsi-Ayadi, M. Treatment of Dye-Containing Effluent by Natural Clay. *J. Clean. Prod.* **2015**, *86*, 432–440. [[CrossRef](#)]
27. Lagaly, G. Colloid Clay Science. In *Developments in Clay Science*; Bergaya, F., Theng, B.K.G., Lagaly, G., Eds.; Elsevier Science: Amsterdam, The Netherlands, 2006; Volume 1, pp. 141–245. ISBN 978-0-08-044183-2.
28. Moreira, M.A.; Ciuffi, K.J.; Rives, V.; Vicente, M.A.; Trujillano, R.; Gil, A.; Korili, S.A.; de Faria, E.H. Effect of Chemical Modification of Palygorskite and Sepiolite by 3-Aminopropyltriethoxysilane on Adsorption of Cationic and Anionic Dyes. *Appl. Clay Sci.* **2017**, *135*, 394–404. [[CrossRef](#)]

29. Middea, A.; Spinelli, L.S.; Souza Jr, F.G.; Neumann, R.; Fernandes, T.L.A.P.; Gomes, O. da F.M. Preparation and Characterization of an Organo-Palygorskite-Fe<sub>3</sub>O<sub>4</sub> Nanomaterial for Removal of Anionic Dyes from Wastewater. *Appl. Clay Sci.* **2017**, *139*, 45–53. [[CrossRef](#)]
30. Chen, H.; Zhong, A.; Wu, J.; Zhao, J.; Yan, H. Adsorption Behaviors and Mechanisms of Methyl Orange on Heat-Treated Palygorskite Clays. *Ind. Eng. Chem. Res.* **2012**, *51*, 14026–14036. [[CrossRef](#)]
31. Zhao, G.; Shi, L.; Feng, X.; Yu, W.; Zhang, D.; Fu, J. Palygorskite-Cerium Oxide Filled Rubber Nanocomposites. *Appl. Clay Sci.* **2012**, *67–68*, 44–49. [[CrossRef](#)]
32. Christoforidis, K.C.; Montini, T.; Fittipaldi, M.; Jaén, J.J.D.; Fornasiero, P. Photocatalytic Hydrogen Production by Boron Modified TiO<sub>2</sub>/Carbon Nitride Heterojunctions. *ChemCatChem* **2019**, *11*, 6408–6416. [[CrossRef](#)]
33. Christoforidis, K.C.; Fornasiero, P. Photocatalytic Hydrogen Production: A Rift into the Future Energy Supply. *ChemCatChem* **2017**, *9*, 1523–1544. [[CrossRef](#)]
34. Gao, Y.; Zheng, Y.; Chai, J.; Tian, J.; Jing, T.; Zhang, D.; Cheng, J.; Peng, H.; Liu, B.; Zheng, G. Highly Effective Photocatalytic Performance of {001}-TiO<sub>2</sub>/MoS<sub>2</sub>/RGO Hybrid Heterostructures for the Reduction of Rh B. *RSC Adv.* **2019**, *9*, 15033–15041. [[CrossRef](#)] [[PubMed](#)]
35. Reza, K.M.; Kurny, A.; Gulshan, F. Parameters Affecting the Photocatalytic Degradation of Dyes Using TiO<sub>2</sub>: A Review. *Appl. Water Sci.* **2017**, *7*, 1569–1578. [[CrossRef](#)]
36. Ling, L.; Wang, Y.; Zhang, W.; Ge, Z.; Duan, W.; Liu, B. Preparation of a Novel Ternary Composite of TiO<sub>2</sub>/UiO-66-NH<sub>2</sub>/Graphene Oxide with Enhanced Photocatalytic Activities. *Catal. Lett.* **2018**, *148*, 1978–1984. [[CrossRef](#)]
37. Papoulis, D.; Panagiotaras, D.; Tsigrou, P.; Christoforidis, K.C.; Petit, C.; Apostolopoulou, A.; Stathatos, E.; Komarneni, S.; Koukouvelas, I. Halloysite and Sepiolite-TiO<sub>2</sub> nanocomposites: Synthesis Characterization and Photocatalytic Activity in Three Aquatic Wastes. *Mater. Sci. Semicond. Processing* **2018**, *85*, 1–8. [[CrossRef](#)]
38. Papoulis, D.; Komarneni, S.; Panagiotaras, D.; Nikolopoulou, A.; Christoforidis, K.C.; Fernández-García, M.; Li, H.; Shu, Y.; Sato, T. Palygorskite-TiO<sub>2</sub> Nanocomposites: Part 2. Photocatalytic Activities in Decomposing Air and Organic Pollutants. *Appl. Clay Sci.* **2013**, *83–84*, 198–202. [[CrossRef](#)]
39. Papoulis, D.; Komarneni, S.; Panagiotaras, D.; Stathatos, E.; Christoforidis, K.C.; Fernández-García, M.; Li, H.; Shu, Y.; Sato, T.; Katsuki, H. Three-Phase Nanocomposites of Two Nanoclays and TiO<sub>2</sub>: Synthesis, Characterization and Photocatalytic Activities. *Appl. Catal. B Environ.* **2014**, *147*, 526–533. [[CrossRef](#)]
40. Gao, L.; Zhang, Q.; Li, J.; Feng, R.; Xu, H.; Xue, C. Adsorption of Methyl Orange on Magnetically Separable Mesoporous Titania Nanocomposite. *Chin. J. Chem. Eng.* **2014**, *22*, 1168–1173. [[CrossRef](#)]
41. Jafari, S.; Sillanpää, M. Adsorption of Dyes onto Modified Titanium Dioxide. In *Advanced Water Treatment*; Elsevier: Amsterdam, The Netherlands, 2020; pp. 85–160.
42. Wu, W.; Yao, T.; Xiang, Y.; Zou, H.; Zhou, Y. Efficient Removal of Methyl Orange by a Flower-like TiO<sub>2</sub> /MIL-101(Cr) Composite Nanomaterial. *Dalton Trans.* **2020**, *49*, 5722–5729. [[CrossRef](#)]
43. Zhao, Y.; Zhang, Q.; Li, Y.; Zhang, R.; Lu, G. Large-Scale Synthesis of Monodisperse UiO-66 Crystals with Tunable Sizes and Missing Linker Defects via Acid/Base Co-Modulation. *ACS Appl. Mater. Interfaces* **2017**, *9*, 15079–15085. [[CrossRef](#)] [[PubMed](#)]
44. Christoforidis, K.C.; Figueroa, S.J.A.; Fernández-García, M. Iron-Sulfur Codoped TiO<sub>2</sub> Anatase Nano-Materials: UV and Sunlight Activity for Toluene Degradation. *Appl. Catal. B Environ.* **2012**, *117–118*, 310–316. [[CrossRef](#)]
45. Zhang, J.; Guo, Z.; Yang, Z.; Wang, J.; Xie, J.; Fu, M.; Hu, Y. TiO<sub>2</sub> @UiO-66 Composites with Efficient Adsorption and Photocatalytic Oxidation of VOCs: Investigation of Synergistic Effects and Reaction Mechanism. *ChemCatChem* **2021**, *13*, 581–591. [[CrossRef](#)]
46. Han, Y.; Liu, M.; Li, K.; Zuo, Y.; Wei, Y.; Xu, S.; Zhang, G.; Song, C.; Zhang, Z.; Guo, X. Facile Synthesis of Morphology and Size-Controlled Zirconium Metal–Organic Framework UiO-66: The Role of Hydrofluoric Acid in Crystallization. *CrystEngComm* **2015**, *17*, 6434–6440. [[CrossRef](#)]
47. Tang, J.; Dong, W.; Wang, G.; Yao, Y.; Cai, L.; Liu, Y.; Zhao, X.; Xu, J.; Tan, L. Efficient Molybdenum<sup>vi</sup> Modified Zr-MOF Catalysts for Epoxidation of Olefins. *RSC Adv.* **2014**, *4*, 42977–42982. [[CrossRef](#)]
48. Zhang, Q.; Yang, T.; Liu, X.; Yue, C.; Ao, L.; Deng, T.; Zhang, Y. Heteropoly Acid-Encapsulated Metal–Organic Framework as a Stable and Highly Efficient Nanocatalyst for Esterification Reaction. *RSC Adv.* **2019**, *9*, 16357–16365. [[CrossRef](#)]
49. Christoforidis, K.C.; Iglesias-Juez, A.; Figueroa, S.J.A.; Newton, M.A.; Michiel, M.D.; Fernández-García, M. A Structural and Surface Approach to Size and Shape Control of Sulfur-Modified Undoped and Fe-Doped TiO<sub>2</sub> Anatase Nano-Materials. *Phys. Chem. Chem. Phys.* **2012**, *14*, 5628–5634. [[CrossRef](#)]
50. Zhu, J.; Zhang, P.; Wang, Y.; Wen, K.; Su, X.; Zhu, R.; He, H.; Xi, Y. Effect of Acid Activation of Palygorskite on Their Toluene Adsorption Behaviors. *Appl. Clay Sci.* **2018**, *159*, 60–67. [[CrossRef](#)]
51. Giustetto, R.; Chiari, G. Crystal Structure Refinement of Palygorskite from Neutron Powder Diffraction. *Eur. J. Mineral.* **2004**, *16*, 521–532. [[CrossRef](#)]
52. Giustetto, R.; Seenivasan, K.; Pellerej, D.; Ricchiardi, G.; Bordiga, S. Spectroscopic Characterization and Photo/Thermal Resistance of a Hybrid Palygorskite/Methyl Red Mayan Pigment. *Microporous Mesoporous Mater.* **2012**, *155*, 167–176. [[CrossRef](#)]
53. Christoforidis, K.C.; Melchionna, M.; Montini, T.; Papoulis, D.; Stathatos, E.; Zafeiratos, S.; Kordouli, E.; Fornasiero, P. Solar and Visible Light Photocatalytic Enhancement of Halloysite Nanotubes/g-C<sub>3</sub>N<sub>4</sub> Heteroarchitectures. *RSC Adv.* **2016**, *6*, 86617–86626. [[CrossRef](#)]

54. Shahriyari Far, H.; Hasanzadeh, M.; Najafi, M.; Rahimi, R. In-Situ Self-Assembly of Mono- and Bi-Metal Organic Frameworks onto Clay Mineral for Highly Efficient Adsorption of Pollutants from Wastewater. *Chem. Phys. Lett.* **2022**, *799*, 139626. [[CrossRef](#)]
55. Hidayat, A.R.P.; Sulistiono, D.O.; Murwani, I.K.; Endrawati, B.F.; Fansuri, H.; Zulfa, L.L.; Ediati, R. Linear and Nonlinear Isotherm, Kinetic and Thermodynamic Behavior of Methyl Orange Adsorption Using Modulated Al<sub>2</sub>O<sub>3</sub>@UiO-66 via Acetic Acid. *J. Environ. Chem. Eng.* **2021**, *9*, 106675. [[CrossRef](#)]
56. Vasiliadou, I.A.; Ioannidou, T.; Anagnostopoulou, M.; Polyzotou, A.; Papoulis, D.; Christoforidis, K.C. Adsorption of Methyl Orange on a Novel Palygorskite/UiO-66 Nanocomposite. *Appl. Sci.* **2022**, *12*, 7468. [[CrossRef](#)]
57. Yang, J.-M. A Facile Approach to Fabricate an Immobilized-Phosphate Zirconium-Based Metal-Organic Framework Composite (UiO-66-P) and Its Activity in the Adsorption and Separation of Organic Dyes. *J. Colloid Interface Sci.* **2017**, *505*, 178–185. [[CrossRef](#)]
58. Chen, Q.; He, Q.; Lv, M.; Xu, Y.; Yang, H.; Liu, X.; Wei, F. Selective Adsorption of Cationic Dyes by UiO-66-NH<sub>2</sub>. *Appl. Surf. Sci.* **2015**, *327*, 77–85. [[CrossRef](#)]
59. Ho, Y.S.; McKay, G. Pseudo-Second Order Model for Sorption Processes. *Process Biochem.* **1999**, *34*, 451–465. [[CrossRef](#)]
60. Yao, P.; Liu, H.; Wang, D.; Chen, J.; Li, G.; An, T. Enhanced Visible-Light Photocatalytic Activity to Volatile Organic Compounds Degradation and Deactivation Resistance Mechanism of Titania Confined inside a Metal-Organic Framework. *J. Colloid Interface Sci.* **2018**, *522*, 174–182. [[CrossRef](#)]
61. Li, F.; Sun, S.; Jiang, Y.; Xia, M.; Sun, M.; Xue, B. Photodegradation of an Azo Dye Using Immobilized Nanoparticles of TiO<sub>2</sub> Supported by Natural Porous Mineral. *J. Hazard. Mater.* **2008**, *152*, 1037–1044. [[CrossRef](#)]